Low-Temperature Structure and Dynamics of Brucite

B. C. Chakoumakos,*,† C.-K. Loong,‡ and A. J. Schultz‡

Solid State Division, Oak Ridge National Laboratory, Oak Ridge, Tennessee 37831, and Intense Pulsed Neutron Source Division, Argonne National Laboratory, Argonne, Illinois 60439

Received: July 9, 1997[⊗]

Structural refinements of time-of-flight neutron powder diffraction data for $Mg(OD)_2$ and inelastic neutron scattering measurements for $Mg(OH)_2$ demonstrate that the mechanism of thermal contraction is primarily the reduction of the octahedral thickness and secondarily the reduction of the interlayer thickness. The contraction of the octahedral layer thickness is 4 times as great as the contraction of the interlayer thickness over the temperature interval 300−15 K. The volume of brucite at 15 K is equivalent to that at 0.2 GPa, which should not be sufficient to observe the H-bonding between the octahedral layer that occurs at high pressure; however, the three-site split-atom model, in which the O−D direction makes an angle α with the 3-fold *c* axis, provides a better fit to the data for each temperature than the single-site model. The O−D distance from the single-site model is markedly shortened by the large atomic displacement parameter of the D atom, but if the O−D distance is corrected for "riding" motion, it lengthens roughly to the same values determined from the three-site split-atom model. The temperature dependence of the lattice parameters are given by $a = 3.1435 + 2.911 \times 10^{-5}T + 9.944 \times 10^{-8}T^2 - 1.965 \times 10^{-11}T^3 - 4.789 \times 10^{-13}T^4$, $c = 4.7478 + 1.793 \times 10^{-4}T + 4.496 \times 10^{-7}T^2 + 3.910 \times 10^{-10}T^3$, $V = 40.635 + 2.330 \times 10^{-3}T + 5.592 \times 10^{-6}T^2 + 1.748 \times 10^{-9}T^3$, for T in °C. The vibrational spectrum of hydrogen in $Mg(OH)_2$ at 15 K obtained from inelastic scattering measurements shows a sharp OH stretch band at 461.8 meV, an E_u OH libration at 47.5 meV, and other broad features due to lattice vibrations and combination excitations. No evidence of enhanced hydrogen bonding was found at low temperatures.

I. Introduction

If the hydrogen atoms are ignored, brucite is isostructural with the layered compound CdI_2 (space group $P\bar{3}m1$). This family of divalent metal hydroxides, $M(OH)_2$, includes M = Mg, Ca, Ni, Co, Fe, Mn, and Cd and consists of layers of edge-sharing octahedra. Because of metal−metal repulsions, the shared edges of the octahedra are shorter than the unshared edges, resulting in a distortion of the octahedra from a regular form. The hydroxyl groups are directed along the layer stacking direction and are bonded to three metal cations. Within the interlayer spacings, the hydroxyl groups are each surrounded by three other hydroxyl groups belonging to the adjacent layer.

The brucite crystal structure is of significance as a model system for the behavior of the hydroxyl bond as a function of intensive conditions and varied metal chemistry. Moreover, the brucite "layer" is a fundamental building unit of a great variety of geologically important hydrous phyllosilicates, which include micas and clays. The nature of the interlayer forces, in the absence of hydrogen bonding, might be considered a contentious issue in these compounds, but this understanding appears to be limited by the resolution of the diffraction experiments to accurately describe the crystal structure. From early studies of $Ca(OH)_2$[1] the large and anisotropic displacement parameters of the hydrogen atom have demanded explanation. Busing and Levy[1] proposed an umbrella-shaped distribution of the hydrogen atom position, in which the H atom undergoes a "riding" motion on the oxygen. Most recently, Desgranges et al.[2,3] have analyzed more extensive single-crystal neutron diffraction data for $Mg(OH)_2$ and $Ca(OH)_2$ with an anharmonic model and with a three-site split-atom model for the H position. They conclude that a model with the H atom displaced from the 3-fold axis is the most realistic. Parise et al.[4] have proposed the same three-site split-atom model to best fit neutron diffraction data for brucite under compression, over the pressure range 0.4−9.3 GPa.

Since the thermal contraction of brucite is large,[5] the temperature dependence of the structural parameters might be similar to the pressure dependence observed for brucite under compression; therefore we have explored the low-temperature structure for similar evidence by means of high-precision structural refinements and inelastic neutron scattering.

II. Methods

The $Mg(OD)_2$ used here was prepared by hydrothermal reaction of optical quality single crystals of MgO with D_2O in an autoclave at 250 °C. This synthesis yields a well-crystallized product. Pulsed neutron powder diffraction data were collected for $Mg(OD)_2$ using the HIPD at the Intense Pulsed Neutron Source, Argonne National Laboratory. The structure was refined using the General Structure Analysis System (GSAS), a Rietveld refinement program developed by Larson and Von Dreele.[6] Data with a *d* spacing range of 0.365−6.0 Å were collected from a 90° detector bank for several temperatures between 15 and 300 K for a sample held in a vanadium can. The neutron scattering lengths for Mg, O, D, and H were taken as $b_{Mg} = 5.38$, $b_O = 5.81$, $b_D = 6.67$, and $b_H = -3.74$ fm. As developed by Partin et al.,[7] a pseudo-Voigt profile function to allow for strain and particle-size broadening was employed in the Rietveld refinements. Models for the ideal structure with anisotropic displacement parameters and with a three-site split-atom and isotropic displacement parameters are refined and compared. In the former model, 23 variables (10 structural + 13 profile and background) were refined, and in the latter model, 22 variables (9 structural + 13 profile and background) were refined. Refinement of the D/H ratio for the 300 K data showed that the sample is 86% deuterated, so this value was held fixed for the refinement of the data for other temperatures. Figure 1

† Oak Ridge National Laboratory.
‡ Argonne National Laboratory.
⊗ Abstract published in *Advance ACS Abstracts,* November 1, 1997.

S1089-5647(97)02225-6 CCC: $14.00

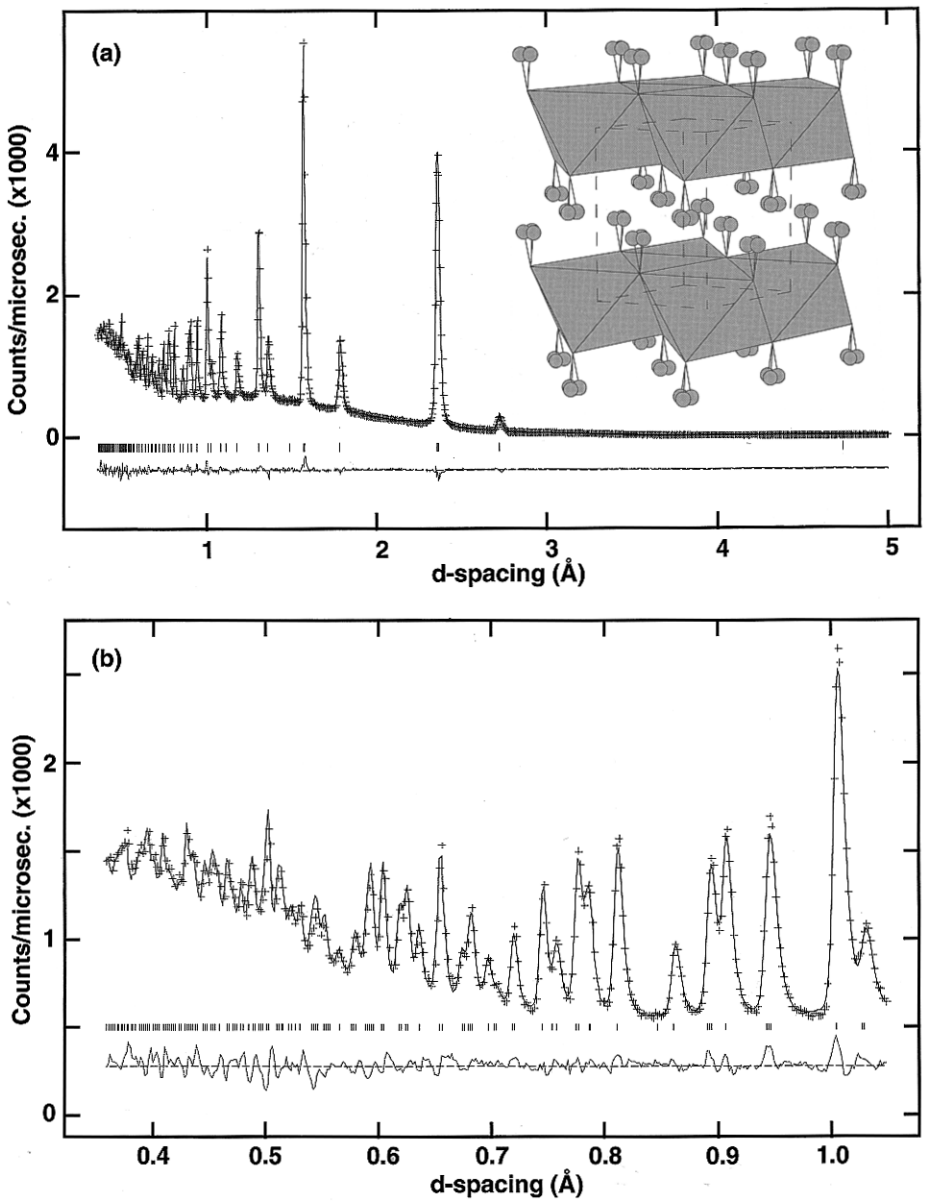

Figure 1. Sample Rietveld analysis fit (solid line) of the TOF neutron powder diffraction data (shown as crosses), 15 K data from HIPD 90° bank at IPNS. The difference curve is shown at the bottom, and the vertical bars mark the reflection positions. (a) Full pattern. (b) Expanded high-Q range. The inset shows a clinographic projection of the brucite, $Mg(OD)_2$, structure, with the three-site split-atom D position. Shaded octahedra are MgO_6. The balls show D positions, which must be one-third occupied.

is a sample Rietveld refinement fit of one data set, with a structure cartoon inset.

By the same method a large volume of $Mg(OH)_2$ (21 g) was also prepared and used to collect inelastic neutron scattering data with the high-resolution medium-energy chopper spectrometer (HRMECS) also at IPNS, ANL.[8] The energy resolution in full width at half-maximum of HRMECS varies from ~4% of the incident energy (E_0) in the elastic region to ~2% near the end of the neutron-energy-loss spectrum. Data were collected at E_0 of 150, 300, and 600 meV so that all the inelastic features from 0 to 500 meV were measured with good resolution. The majority of the data were obtained at 15 K to avoid background due to excessive multiple-phonon scattering. Since the scattering cross section of H is more than 10 times larger than those of Mg and O, the spectra are dominated by scattering which involves H motion.

III. Results

Two structural models were refined and are compared. The first model employed was the ideal structure, with the D atom situated on the 3-fold axis. For this model, anisotropic atomic displacement parameters (ADPs) for the O and D atoms were used. The Mg ADP tended to become nonpositive definite so it was kept isotropic. The second model was the three-site split-atom structure proposed by Desgranges et al.,[2] with isotropic ADPs used for all the atoms. The structural description and refinement results are given in Tables 1 and 2. The three-site split-atom model, in which the O−D direction makes an angle α with the 3-fold c axis, provides a better fit to the data for each temperature than the single-site model. The O−D distance

TABLE 1: Crystal Structural Parameters for Brucite, $Mg(OD)_2$

space group: $P\bar{3}m1$					
For each atom, $u_{22} = u_{11}$, $u_{12} = u_{11}/2$, $u_{13} = u_{23} = 0$					
T factor $= \exp[-2\pi^2(u_{11} - h^2a^{*2} + ... + 2u_{12}hka^*b^* + ...)]$					
Mg	1*a*	3*m*	0	0	0
O	2*d*	3*m*	1/3	2/3	z_O
D	2*d*	3*m*	1/3	2/3	z_D
In the three-site split-atom model, the D position is					
D	6*i*	3*m*	x	2x	z_D
and 1/3 occupied					

TABLE 2: Rietveld Refinement Results for Brucite, $Mg(OD)_2$, Using IPNS HIPD 90° Bank TOF Neutron Diffraction Data

T (K)	χ^2	R_{wp} (%)	*a* (Å)	*c* (Å)	*V* (Å^3)	*U* (Å^2) (Mg)	*z* (O)	$\langle u_1^2 \rangle$ (O)	$\langle u_3^2 \rangle$ (O)	*U* (Å^2) (O)	x (D)	*z* (D)	$\langle u_1^2 \rangle$ (D)	$\langle u_3^2 \rangle$ (D)	*U* (Å^2) (D)
15	3.18	3.49	3.14080(8)	4.7270(2)	40.383(3)	0.07(2)	0.2184(2)	0.28(2)	0.41(5)	0.32		0.4207(2)	1.20(4)	0.20(6)	0.87
	2.53	3.87	3.14082(7)	4.7270(2)	40.383(2)	−0.02(1)	0.2187(2)			0.42(2)	0.3610(4)	0.4209(2)			0.21(3)
45	2.56	3.89	3.14081(7)	4.7277(2)	40.389(2)	−0.01(2)	0.2186(2)	0.26(2)	0.48(4)	0.34		0.4210(2)	1.15(3)	0.20(5)	0.84
	2.51	3.87	3.14081(7)	4.7277(2)	40.389(2)	−0.02(1)	0.2187(2)			0.40(2)	0.3606(4)	0.4209(2)			0.24(3)
75	2.52	3.86	3.14099(7)	4.7294(2)	40.409(2)	0.01(2)	0.2183(2)	0.22(2)	0.47(5)	0.31		0.4212(2)	1.17(3)	0.24(5)	0.86
	2.46	3.82	3.14100(7)	4.7294(2)	40.409(2)	−0.05(1)	0.2185(2)			0.40(2)	0.3599(4)	0.4213(2)			0.27(3)
105	2.42	3.79	3.14102(7)	4.7310(2)	40.423(2)	−0.02(3)	0.2186(2)	0.32(3)	0.54(5)	0.39		0.4215(2)	1.13(4)	0.24(5)	0.84
	2.36	3.76	3.14102(7)	4.7309(2)	40.422(2)	−0.00(1)	0.2186(2)			0.43(2)	0.3604(4)	0.4214(2)			0.27(3)
135	2.35	3.74	3.14109(7)	4.7333(2)	40.444(2)	0.00(2)	0.2185(2)	0.36(3)	0.65(5)	0.46		0.4209(2)	1.24(4)	0.29(6)	0.93
	2.30	3.71	3.14109(7)	4.7332(2)	40.444(2)	0.01(1)	0.2186(2)			0.52(2)	0.3610(4)	0.4209(2)			0.34(3)
165	2.22	3.62	3.14144(7)	4.7358(2)	40.475(2)	−0.03(2)	0.2187(2)	0.40(3)	0.75(5)	0.52		0.4208(2)	1.29(4)	0.30(5)	0.97
	2.18	3.60	3.14144(7)	4.7357(2)	40.474(2)	−0.01(1)	0.2188(2)			0.60(2)	0.3611(4)	0.4207(2)			0.38(3)
195	2.21	3.60	3.14194(7)	4.7390(2)	40.515(2)	0.02(2)	0.2191(2)	0.44(3)	0.79(6)	0.56		0.4207(2)	1.43(5)	0.35(6)	1.07
	2.16	3.57	3.14194(7)	4.7389(2)	40.514(2)	−0.00(1)	0.2192(2)			0.67(2)	0.3622(4)	0.4207(2)			0.41(4)
225	2.06	3.50	3.14236(7)	4.7426(2)	40.556(2)	0.08(3)	0.2187(2)	0.51(3)	0.88(6)	0.64		0.4198(3)	1.53(5)	0.48(6)	1.18
	2.04	3.50	3.14237(7)	4.7425(2)	40.556(2)	0.05(2)	0.2188(2)			0.76(3)	0.3618(5)	0.4198(2)			0.57(4)
255	1.98	3.43	3.14310(7)	4.7470(2)	40.614(2)	0.09(3)	0.2191(2)	0.56(3)	0.98(6)	0.70		0.4197(3)	1.63(5)	0.53(7)	1.27
	1.96	3.41	3.14311(7)	4.7469(2)	40.613(2)	0.07(2)	0.2193(2)			0.84(3)	0.3626(5)	0.4198(3)			0.61(4)
285	1.91	3.36	3.14377(7)	4.7515(2)	40.670(2)	0.18(3)	0.2190(3)	0.53(3)	1.08(7)	0.72		0.4189(3)	1.81(5)	0.52(7)	1.39
	1.89	3.36	3.14379(7)	4.7514(2)	40.669(2)	0.11(2)	0.2193(2)			0.88(3)	0.3632(5)	0.4191(3)			0.69(4)
300	1.57	3.91	3.14413(8)	4.7541(2)	40.701(3)	0.16(4)	0.2194(3)	0.56(4)	1.13(8)	0.76		0.4192(3)	1.88(7)	0.59(9)	1.46
	1.56	3.91	3.14414(8)	4.7540(2)	40.701(3)	0.12(2)	0.2197(3)			0.91(3)	0.3637(6)	0.4193(3)			0.75(5)

[a] All atomic displacement parameter values to be multiplied by 10^{-2} Å^2. For each temperature the first entry is the single-site model with anisotropic ADPs for O and D, and the second entry is the three-site model with isotropic ADPs.

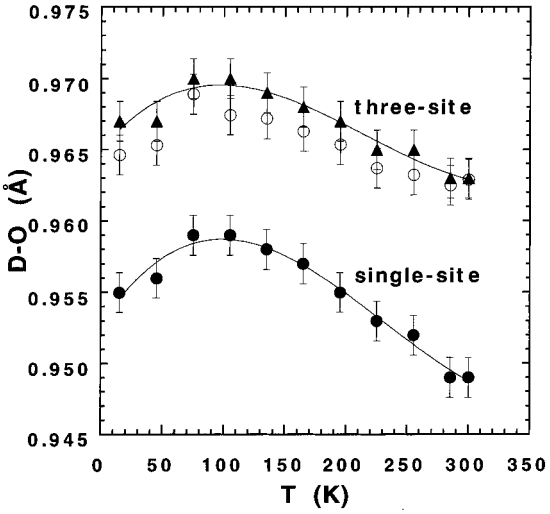

Figure 2. Interatomic D−O distances as a function of temperature. The full circles show the single-site model uncorrected for the large D atom motion, and the open circles show the same distances corrected for the large thermal motion of the D atom by $d(DO)_{corrected} = d(DO) + (\langle u_D^2 \rangle - \langle u_O^2 \rangle)/d(DO)$, where *u*'s are the displacements normal to the bond. The triangles are from the three-site split-atom model.

from the single-site model is markedly shortened by the large ADP of the D atom (Figure 2); but if the O−D distances are corrected for the "riding" motion in a manner as suggested by Busing and Levy,[1] they lengthen roughly to the same values determined from the three-site split-atom model.

Brucite is often used in determining geologically relevant equilibria reactions of minerals. Therefore, accurate estimates of its thermal expansion are useful, particularly since the thermal expansion is large. The thermal expansion of brucite was evaluated by Redfern and Wood[7] over the temperature interval 20−310 °C on the basis of XRD data. We have the opportunity now to further constrain the thermal expansion of brucite by combining our new low-temperature measurements with their cell data. In merging the data, systematic errors in the lattice parameters were evident. To make the combined data (*a*, *c*, and *c*/*a*) vary smoothly, 0.005 Å was subtracted from the *a* values of Redfern and Wood,[9] and 0.0023 Å was added to the *c* values of this study. The least-squares analysis of the temperature dependence of the lattice parameters using polynomials gives the following:

$$a = 3.1435 + 2.911 \times 10^{-5}T + 9.944 \times 10^{-8}T^2 - 1.965 \times 10^{-11}T^3 - 4.789 \times 10^{-13}T^4 \pm 0.0005 \text{ Å}$$

$$c = 4.7478 + 1.793 \times 10^{-4}T + 4.496 \times 10^{-7}T^2 + 3.910 \times 10^{-10}T^3 \pm 0.003 \text{ Å}$$

$$V = 40.635 + 2.330 \times 10^{-3}T + 5.592 \times 10^{-6}T^2 + 1.748 \times 10^{-9}T^3 \pm 0.02 \text{ Å}^3$$

where the temperature is in °C. Using these expressions the instantaneous isobaric thermal expansion can be approximated as $\alpha_x = (1/x_0)(\partial x/\partial T)p$, where x_0 is a reference lattice constant at T_0 °C. The improved T_0 values are $\alpha_1 = 9.26 \times 10^{-6}$, $\alpha_3 = 3.77 \times 10^{-5}$, and $\alpha_{vol} = 5.73 \times 10^{-5}$.

The manner by which the structure accommodates thermal contraction is not what is expected. The larger interlayer distance shows a small but steady contraction with decreasing temperature, but the smaller octahedral layer thickness contracts 4 times as much over two-thirds of the temperature interval (Figure 3). Below 100 K the octahedral layer thickness remains constant.

Figure 4 displays excitation spectra of $Mg(OH)_2$ at 15 K obtained from HRMECS using incident neutron energies of 150 and 600 meV. The 150−400 meV region does not show any distinct sharp features. The layered structure of brucite gives rise to fundamental vibrational modes which may be loosely grouped as lattice vibrations in 0−60 meV, OH librations in 40−90 meV, and OH stretches in 450−460 meV. In addition, there are sharp combination bands due to multiple excitations of distinct fundamental modes as well as a weak diffuse background due to higher order combinations. Unlike Raman and infrared spectroscopy, neutron scattering from atoms in crystalline materials is not restricted by selection rules. Moreover, neutrons probe lattice vibrations throughout the Brillouin zone, whereas Raman or IR measurements reveal only the energies of the zone center modes. When comparing neutron and optical spectroscopy data, the normally sharp Raman or IR features may correspond to broader phonon bands due to

TABLE 3: Selected Interatomic Distances and Angles for Brucite, $Mg(OD)_2$

T (K)	Mg−O (Å)	O−Mg−O (deg)	O···O (Å)	oct. layer (Å)	interlayer (Å)	H···H (Å)	H···H (Å)	α (deg)	O−H···O (deg)
15	2.0874(5)	82.41(3)	3.218(1)	2.067(2)	2.659(2)	0.261(4)	1.896(2)	8.9(1)	144.6(1) 126.5(2)
45	2.0874(5)	82.41(3)	3.219(1)	2.067(2)	2.660(2)	0.260(4)	1.896(2)	8.9(1)	144.6(2) 126.6(2)
75	2.0872(5)	82.39(3)	3.221(1)	2.066(2)	2.662(2)	0.250(4)	1.897(2)	8.5(1)	144.1(2) 126.9(2)
105	2.0876(5)	82.42(3)	3.221(1)	2.068(2)	2.662(2)	0.255(4)	1.896(2)	8.7(1)	144.3(1) 126.7(2)
135	2.0877(6)	82.42(3)	3.223(1)	2.068(2)	2.664(2)	0.250(4)	1.898(2)	8.5(1)	144.1(2) 126.9(2)
165	2.0888(6)	82.47(3)	3.222(1)	2.072(2)	2.663(2)	0.262(4)	1.897(2)	8.9(1)	144.7(2) 126.6(2)
195	2.0906(6)	82.55(3)	3.220(1)	2.077(2)	2.661(2)	0.272(4)	1.896(2)	9.3(1)	145.1(2) 126.3(2)
225	2.0900(6)	82.51(3)	3.225(2)	2.075(2)	2.667(2)	0.268(5)	1.900(3)	9.2(1)	145.1(2) 126.5(2)
255	2.0921(6)	82.61(3)	3.224(2)	2.081(2)	2.664(2)	0.276(5)	1.899(2)	9.5(1)	145.5(2) 126.2(2)
285	2.0921(7)	82.63(4)	3.226(2)	2.083(2)	2.667(2)	0.281(5)	1.901(3)	9.7(1)	145.8(2) 126.1(2)
300	2.0943(7)	82.70(4)	3.224(2)	2.088(2)	2.665(2)	0.286(6)	1.899(3)	9.8(2)	146.0(2) 125.9(3)

TABLE 4: Vibrational Mode Assignments (meV) for $Mg(OH)_2$ and $[Mg(OD)_2]$ at Room Temperature (Unless Otherwise Noted), Neglecting the Coupling between Librational and Translational Vibrations, after Lutz et al.[19] The Second Line Gives Mean Values, and OD Bands Are in Brackets

stretching modes *n*OH [*n*OD]		librations R		lattice vibrations T′				
A_{1g} (Raman)	A_{2u} (IR)	E_g (Raman)	E_u (IR)	A_{1g}	A_{2u}	E_g	E_u	references
452.7 [334.2]	457.2	89.8 [62.7]	51.5	54.9 [53.8]	54.9	34.7 [34.3]	44.7	16[b]
453.0 [334.2]	458.4 [337.2]	89.8 [62.7]	51.4	55.0 [53.8]	56.4	34.7 [34.3]	45.2	16−18, 20−22
468[a]			47.5[a]		see text			present work

[a] 15 K. [b] IR and Raman single-crystal data.

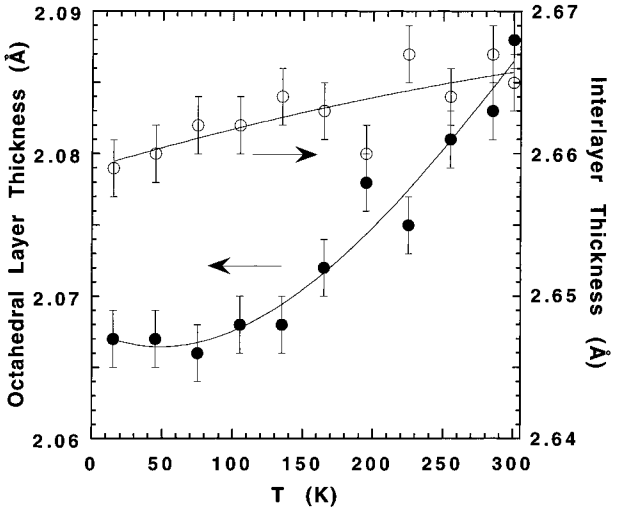

Figure 3. Octahedral layer thickness and interlayer thickness as a function of temperature.

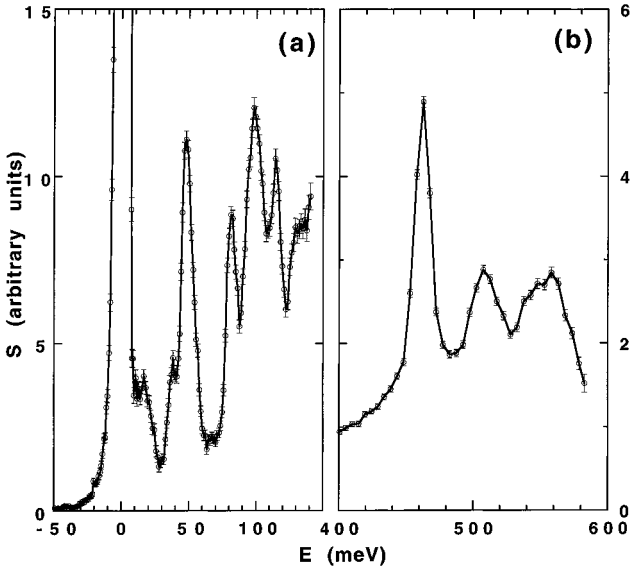

Figure 4. Observed vibrational spectra of $Mg(OH)_2$ at 15 K obtained from the HRMECS measurements with incident neutron energies of (a) 150 and (b) 600 meV. The bands centered at 15.6, 47.5, and 461.8 meV arise from acoustic phonons, E_u OH libration, and OH stretches, respectively. The remaining fundamental modes cannot be separated unambiguously from the higher order multiple excitations (see text).

dispersion relations, and the peak positions may not coincide except for nondispersive internal modes. Because of the much larger scattering cross section of H, the measured inelastic spectrum obtained from HRMECS can effectively be regarded as a measure of the vibrational density of states of the hydrogen atoms.

Inelastic neutron scattering studies of the low-energy (0−80 meV) vibrational modes of brucite at room temperature have been carried out by Safford et al.[10] and by Pelah et al.[11] The peaks at 15.6, 38, 47.5, and 81.3 meV in Figure 4a agree well with the previous results albeit with small energy shifts due to temperature effects. The Raman and IR energies of the fundamental modes and their assignments determined by previous workers are listed in Table 4, and the modes are illustrated in Figure 5. The OH symmetric and antisymmetric stretch vibrations, which are separated by ∼5.6 meV, are not resolved by the neutron measurement. Such a small splitting is indicative of a relatively regular force field of the $M\cdots OH^-$ environment and negligible hydrogen bonding.[12] In the case of ice, boehmite, and newberyite, hydrogen bonding leads to a downshift of the OH stretch energies and a profile skewed toward the lower energy side of the peak.[13] Under high pressure, the Raman active A_{1g} stretch mode of brucite and portlandite shifts toward lower energies, which is attributed to enhanced hydrogen bonding.[14,15]

A strong peak at 47.5 meV and a broad band center around 15.6 meV (see Figure 4a) can be identified as the E_u libration and acoustic phonons, respectively. The remaining E_g libration and the lattice modes ranging from 30 to 100 meV are obscured by a cluster of strong combination bands over the 80−150 meV region. Combination modes of brucite, particularly in the vicinity of the stretch vibrations, have been studied extensively by many authors.[10,11,16−18] Qualitatively, we may assign the peak centered at 509 meV as OH stretch + E_u libration and the peak around 552 meV as OH stretch + $2E_u$ librations. Similarly, the peak at ∼97 meV may be $2E_u$ librations, and the side peaks at 115 and 132 meV may be $2E_u$ + lattice modes. The overlapping of strong combination bands with fundamental

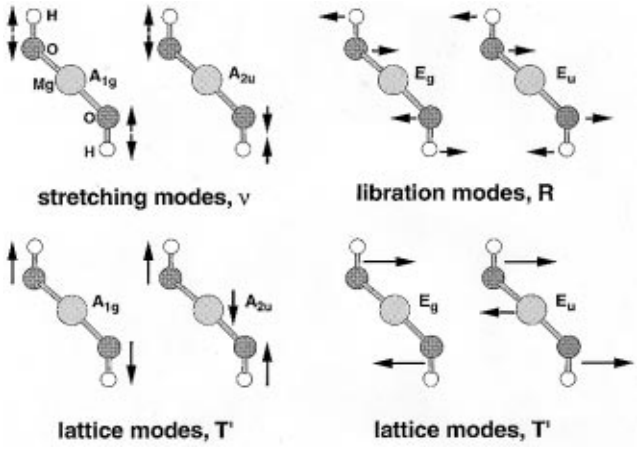

Figure 5. Vibrational modes of brucite, after Lutz et al.[19]

modes in both hydrogenous and deuterated samples has made the quantitative analysis of atomic vibrations in brucite-type hydroxides difficult despite numerous spectroscopic studies.[19] Clearly, more detailed studies are needed to better understand the lattice dynamics and associated phenomena.

IV. Discussion

The variations of the positional parameters, anisotropic ADPs, and α angle with temperature all show changes in slope between 15 and 75 K. For instance, the α angle decreases from 300 to 75 K, then it abruptly begins to increase upon further cooling. For brucite under pressure[4] the α angle increases from 10° to 21° for the pressure change of 0.4 to 9.3 GPa. These results suggest that as brucite is cooled, the initial contraction of the interlayer spacing accommodating the wobbling O−D vector restricts their direction to be closer to the *c* axis. Below about 100 K, however, the interlayer contraction is sufficient to change the interlayer potential such that further contraction of the interlayer spacing causes the α angle to increase, analogous to the behavior at high pressure. It is possible that above 100 K the D positions are dynamically disordered over the three sites, and below 100 K they are statically disordered; however, elastic measurements cannot confirm this idea. Moreover, we do not expect any substantial effect on the vibrational spectra of the present study at low temperatures and relatively high energies. Theoretical assessment of the dynamic response of H disorder or tunneling will be helpful for the design of specific experimental investigation of this structural behavior.

The mechanism of thermal contraction appears to be primarily accommodated by the reduction of the octahedral thickness and secondarily by the reduction of the interlayer thickness. Indeed, the contraction of the octahedral layer thickness is 4 times as great as the contraction of the interlayer thickness over the temperature interval 300−15K (Figure 3). The volume of brucite at 15 K is equivalent to that at 0.2 GPa, which should not be sufficient to observe H-bonding; however, the displaced split-D atom model does improve the refinement results. No hydrogen bonding was indicated at low temperatures on the basis of these elastic and inelastic neutron scattering measurements.

Acknowledgment. This research at Oak Ridge National Laboratory and Argonne National Laboratory was supported by the Division of Materials Sciences, U.S. DOE (Contract DE-AC05-96OR22464 with Lockheed Martin Energy Research Corporation) and by the U.S. DOE-BES (Contract W-31-109-ENG-38 with the University of Chicago), respectively.

References and Notes

(1) Busing, W. R.; Levy, H. A. *J. Chem. Phys.* **1957**, *26*, 563.
(2) Desgranges, L.; Grebille, D.; Galvarin, G.; Chevrier, G.; Floquet, N.; Niepce, J.-C. *Acta Crystallogr.* **1993**, *B49*, 812.
(3) Desgranges, L.; Galvarin, G.; Chevrier, G. *Acta Crystallogr.* **1996**, *B52*, 82.
(4) Parise, J. B.; Leinenweber, K.; Weidner, D. J.; Tan, K.; Von Dreele, R. B. *Am. Mineral.* **1994**, *79*, 193.
(5) Megaw, H. D. *Proc. R. Soc. London* **1933**, *A142*, 198.
(6) Larson, A. C.; Von Dreele, R. B. Los Alamos National Laboratory Report LAUR 86-748, 1986.
(7) Partin, D. E.; O'Keeffe, M.; Von Dreele, R. B. *J. Appl. Crystallogr.* **1994**, *27*, 581.
(8) Loong, C.-K.; Ikeda, S.; Carpenter, J. M. *Nucl. Instrum. Methods* **1987**, *A280*, 381.
(9) Redfern, S. A. T.; Wood, B. J. *Am. Mineral.* **1992**, *77*, 1129.
(10) Safford, G.; Brajovic, V.; Boutin, H. *J. Phys. Chem. Solids* **1963**, *24*, 771.
(11) Pelah, I.; Krebs, K.; Imry, Y. *J. Chem. Phys.* **1965**, *43*, 1864.
(12) Farmer, V. C. *The Infrared Spectra of Minerals*; Mineralogical Society: London, 1974; Chapters 9 and 20.
(13) Loong, C.-K. Unpublished.
(14) Kruger, M. B.; Williams, Q.; Jeanloz, R. *J. Chem. Phys.* **1989**, *91*, 5910.
(15) Duffy, T. S.; Meade, C.; Fei, Y.; Mao, Ho-K.; Hemley, R. J. *Am. Mineral.* **1995**, *80*, 222.
(16) Dawson, P.; Hadfield, C. D.; Wilkinson, G. R. *J. Phys. Chem. Solids* **1973**, *34*, 1217.
(17) Mitra, S. S. *Solid State Phys.* **1962**, *13*, 1.
(18) Buchanan, R. A.; Caspers, H. H.; Murphy, J. *Appl. Opt.* **1963**, *2*, 1147.
(19) Lutz, H. D.; Möller, H.; Schmidt, M. *J. Mol. Struct.* **1994**, *328*, 121.
(20) Cabannes-Ott, C. *Ann. Chim. (Paris)* **1960**, *5*, 905.
(21) Oehler, O.; Gunthard, H. H. *J. Chem. Phys.* **1968**, *48*, 2036.
(22) Martens, R.; Freund, F. *Phys. Status Solidi* **1976**, *A37*, 97.